

# Risk Controlled Image Retrieval

Kaiwen Cai<sup>1</sup>, Chris Xiaoxuan Lu<sup>2</sup>, Xingyu Zhao<sup>3</sup>, Xiaowei Huang<sup>1</sup>

<sup>1</sup>University of Liverpool, <sup>2</sup>University of Edinburgh, <sup>3</sup>University of Warwick

## Abstract

Most image retrieval research focuses on improving predictive performance, ignoring scenarios where the reliability of the prediction is also crucial. Uncertainty quantification technique can be applied to mitigate this issue by assessing uncertainty for retrieval sets, but it can provide only a heuristic estimate of uncertainty rather than a *guarantee*. To address these limitations, we present Risk Controlled Image Retrieval (RCIR), which generates retrieval sets with coverage guarantee, i.e., retrieval sets that are guaranteed to contain the true nearest neighbors with a predefined probability. RCIR can be easily integrated with existing uncertainty-aware image retrieval systems, agnostic to data distribution and model selection. To the best of our knowledge, this is the first work that provides coverage guarantees for image retrieval. The validity and efficiency of RCIR are demonstrated on four real-world image retrieval datasets: Stanford CAR-196, CUB-200, Pittsburgh and ChestX-Det.

## 1 Introduction

Given a query image, the goal of an image retrieval system is to find the best matching candidates from the database. Image retrieval has paved the foundation for many computer vision applications, including face recognition (Cheng and Wang 2019), large-scale image classification (Warburg et al. 2021) and person re-identification (Yao et al. 2019).

An image retrieval system works by representing each image as a vector in a high-dimensional space and finding the nearest neighbors of the query image in the database. Therefore, building discriminative image representations is crucial. Massive research has been devoted to improving the representation power of image features, spanning from early hand-crafted features to nowadays deep learning-based ones (Dubey 2022). However, like other deep learning-based applications, current image retrieval systems are black-box and data-driven. This renders them potentially unreliable due to limited training data and high model complexity.

Meanwhile, reliability is essential for safety-critical applications ranging from autonomous driving to medical diagnosis, where it is vital to be aware of any potential risk associated with the prediction. In the field of medical diagnosis, for instance, the user needs more than just a list of the best-matching candidates from disease databases. Instead, what they prefer or require is a cluster of retrieval results with a

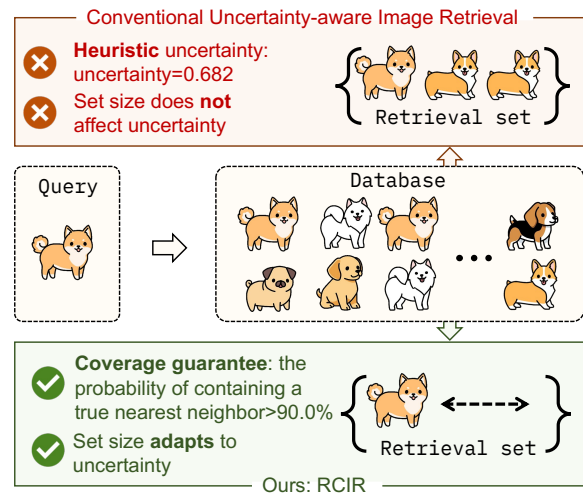


Figure 1: Illustration of RCIR and a conventional uncertainty-aware image retrieval system (e.g., (Warburg et al. 2021)): A conventional uncertainty-aware image retrieval provides a heuristic uncertainty, and has a fixed retrieval set size. In contrast, RCIR provides a retrieval set that is guaranteed to cover a true nearest neighbor with a user-specified risk requirement, while the retrieval size adapts to the uncertainty of the query sample.

specific level of risk<sup>1</sup>, before concluding a diagnosis. Conventional image retrieval systems are inadequate for these tasks as they do not provide any measure for risk control.

Uncertainty estimation has emerged as a risk measure for image retrieval systems. This concept involves estimating the level of uncertainty for both query and database samples. Approaches including (Warburg et al. 2021; Chang et al. 2020; Zhang, Wang, and Deng 2021) use high uncertainty as a signal of potentially inaccurate predictions. However, there are limitations to the uncertainty-aware image retrieval systems. First, the estimated uncertainty is merely a heuristic measure (Angelopoulos et al. 2022) rather than a guarantee.

<sup>1</sup>The risk is defined as the probability of the retrieval set missing all true nearest neighbors of the query samples. Please see Sec.3.3 for a formal definition.

This leaves end users with only an *approximate* understanding of the prediction’s risk. Second, the estimated uncertainty does not consider the retrieval set size. This means that even if there are more candidates in the retrieval set, which increases the chances of including the correct answer, the estimated uncertainty remains unaffected.

These limitations motivate us to propose a novel image retrieval system called Risk Controlled Image Retrieval (RCIR). Fig. 1 highlights the advantages of RCIR compared to conventional uncertainty-aware image retrieval systems (please see the caption for an explanation). Specifically, RCIR uses two modules, the Retrieval Set Size Adapter (Adapter) and the Risk Controller (Controller), to generate retrieval sets that meet a user-specified risk requirement<sup>1</sup>. The Controller calculates the scale  $\kappa$  offline, which is used to guide the Adapter to adjust the size of a retrieval set during inference. This collaboration enables the generation of a risk-controlled retrieval set. We summarize the contributions of this paper as follows:

1. We for the first time utilize the common heuristic uncertainty in a statistical manner to dynamically adjust the retrieval set size.
2. We for the first time allow an image retrieval system to generate retrieval sets that meet a user-specified risk requirement.
3. We demonstrate the effectiveness of RCIR by experimental results on four image retrieval datasets: Stanford CAR-196, CUB-200, Pittsburgh and ChestX-Det.
4. The code of RCIR will be released upon publication.

## 2 Related Work

### 2.1 Image Retrieval

Image retrieval involves building a tagged database offline and searching it online, where images are represented by feature vectors. Therefore, image retrieval’s effectiveness relies on the feature extractor’s representation power. Initially, hand-crafted image features such as SIFT (Lowe 1999) were primarily used. However, with the superior performance of deep learning-based features from pretrained CNNs (Babenko et al. 2014), hand-crafted features have become gradually obsolete. Recent research on image retrieval demonstrates that deep learning-based features can be effectively learned end-to-end with ranking loss functions (Hadsell, Chopra, and LeCun 2006; Schroff, Kalenichenko, and Philbin 2015; Sohn 2016). In this sense, image retrieval has evolved into a metric learning problem, with the aim of learning a mapping function that creates an embedding space where similar objects are positioned close together while dissimilar objects farther apart. Loss functions, including contrastive loss (Hadsell, Chopra, and LeCun 2006),

<sup>1</sup>The risk requirement for this paper involve two factors: the risk level, denoted as  $\alpha$ , and the error rate, denoted as  $\delta$ . The risk requirement asks for a retrieval set that has at least one true nearest neighbor with a probability of  $1 - \alpha$ , and that the chance of the assert fail is limited to  $\delta$ .

triplet loss (Schroff, Kalenichenko, and Philbin 2015), N-pairs loss (Sohn 2016), etc., have been studied to enhance metric learning, which in turn benefits image retrieval.

### 2.2 Uncertainty Estimation

Deep learning has achieved tremendous success in numerous computer vision tasks, but its black-box working mechanism has raised concerns about its reliability. Uncertainty estimation is a way to quantify the confidence of the model in its prediction. Uncertainty of predictions can arise from either the data’s inherent uncertainty or the model’s uncertainty, known as aleatoric and epistemic uncertainty, respectively (Kendall and Gal 2017). To quantify epistemic uncertainty, Variational Inference-based methods such as Monte Carlo Dropout (MCD) are used to approximate Bayesian Neural Networks (BNNs), where the weights of the networks are modeled as distributions. Ensemble method (Fort, Hu, and Lakshminarayanan 2019) initiates multiple instances of the same model and then takes the variances of predictions as an uncertainty level. On the other hand, researchers typically estimate aleatoric uncertainty by learning it via an additional head parallel to the network.

In image retrieval, DUL (Chang et al. 2020) learns aleatoric uncertainty by constructing a stochastic embedding space where the uncertainty is regularized by a KL divergence loss. BTL (Warburg et al. 2021) utilizes a Bayesian loss function that enforces triplet constraints on stochastic embeddings. (Taha et al. 2019) shows MCD can be employed in image retrieval to quantify epistemic uncertainty. Current research on uncertainty estimation in image retrieval is primarily concerned with quantifying the likelihood of a pair of images being similar or dissimilar, albeit with only a heuristic estimate of uncertainty (Angelopoulos et al. 2022). Our objective is to retrieve a set of images guaranteed to contain the true nearest neighbors of a given query sample with a user-specified risk requirement.

The framework of conformal prediction guarantees the correctness of a prediction (Vovk, Gammerman, and Shafer 2005). Conformal quantile regression (Romano, Patterson, and Candes 2019) enhances this approach to deliver prediction intervals with guaranteed accuracy. Building on this idea, DFUQ (Angelopoulos et al. 2022) proposes generating risk-guaranteed intervals in image regression, which motivates us to tackle the constraints of existing image retrieval methods. However, it is important to note that DFUQ is specifically designed for regression tasks that rely on true labels, while our image retrieval approach learns image embeddings without the use of true labels. Furthermore, the uncertainty estimation methods for regression tasks are distinct from those used in image retrieval since true labels are not available (Chang et al. 2020). These differences make it challenging to provide a risk-guaranteed retrieval set in image retrieval, emphasizing the need for a new methodology.

## 3 Method

Fig. 2 illustrates the workflow of a conventional uncertainty-aware image retrieval system (Warburg et al. 2021) and our RCIR. The conventional uncertainty-aware image retrieval

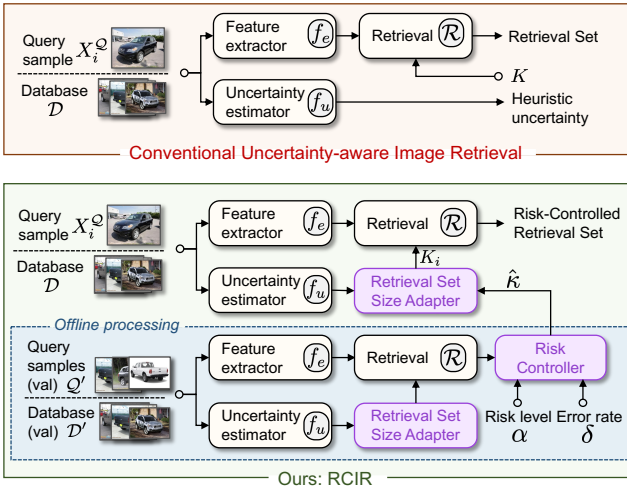


Figure 2: The diagrams of a conventional image retrieval system and our RCIR: Purple blocks  $\square$  (i.e., Retrieval Set Size Adapter and Risk Controller) highlight our contributions. Please see the text below for detailed illustration.

system first uses the feature extractor  $f_e$  to map the query and database samples to embeddings, then the retrieval function  $\mathcal{R}$  obtains the retrieval set, which are the  $K$  nearest neighbors of the query sample in the embedding space. The uncertainty estimator  $f_u$  provides a heuristic uncertainty for each query sample. Our RCIR differs from the conventional one in that the retrieval set is risk-controlled: In the offline processing phase, given the predefined risk requirements, i.e., the risk level  $\alpha$  and the error rate  $\delta$ , we first use the Controller to evaluate the risk of  $\mathcal{R}$  under various  $\kappa$  hypothesis and determine the best scale denoted as  $\hat{\kappa}$ . Then during inference, the Adapter generates the retrieval set size  $K_i$  for the current query sample. In this section, we describe each module in Fig. 2.

### 3.1 Image Retrieval

In an image retrieval system, a feature extractor  $f_e$  is trained to map high-dimensional images to a lower-dimensional embedding space. Similar samples are positioned closely together in this space, while dissimilar samples are positioned far apart. Suppose there is a dataset  $\{\mathcal{Q}, \mathcal{D}\}$ , where  $\mathcal{Q}$  denotes the query set and  $\mathcal{D}$  the database. And given  $i^{\text{th}}$  query sample  $X_i^{\mathcal{Q}} \in \mathcal{Q}$  (superscript denotes which set it belongs to), its most similar samples  $\{Y_{i,j} | j = 1, 2, \dots, K\}$  are retrieved from  $\mathcal{D}$  as

$$\{Y_{i,j} | j = 1, 2, \dots, K\} = \mathcal{R}_{[K, f_e]}(X_i^{\mathcal{Q}}), \quad (1)$$

where  $\mathcal{R}_{[K, f_e]}$  represents a retrieval function conditioned on  $K$  and  $f_e$ :

$$\begin{aligned} \mathcal{R}_{[K, f_e]}(X_i^{\mathcal{Q}}) = \{x | x \in \mathcal{P}, \mathcal{P} \subseteq \mathcal{D}, |\mathcal{P}| = K, \\ d[f_e(X_i^{\mathcal{Q}}), f_e(x)] \leq d[f_e(X_i^{\mathcal{Q}}), f_e(y)], \\ \forall y \in \mathcal{D} \setminus \mathcal{P}\}, \end{aligned} \quad (2)$$

where  $d$  denotes a distance metric function, and  $K$  denotes the number of the retrieved candidates,  $f_e$  denotes the feature extractor. The above image retrieval system has been the *de facto* standard in the image retrieval community. However, it only provides a list of best-matching candidates without indicating their reliability. This lack of reliability information can be problematic in risk-sensitive scenarios where the reliability of the predictions is crucial.

### 3.2 Uncertainty-aware Image Retrieval

Uncertainty estimation techniques mitigate this issue by providing a heuristic uncertainty for each query and database sample. Existing uncertainty-aware image retrieval systems include three methodologies: 1) estimate model uncertainty by BNNs (Gal and Ghahramani 2016), 2) predict uncertainty by a deterministic model (Warburg et al. 2021), and 3) estimate uncertainty by an ensemble of models. Since RCIR utilizes heuristic uncertainty, we briefly introduce them.

**Uncertainty Estimated by a BNN** Bayesian approaches treat the weights of a neural network as distributions instead of as deterministic values. Since obtaining the analytical posterior distribution for the weights is intractable due to the difficulty of acquiring evidence, researchers have utilized various methods to address this challenge, with variational inference being the most widely employed, e.g., Monte Carlo Dropout (MCD) (Gal and Ghahramani 2016). MCD assumes a mixed Gaussian distribution on each weight, which makes the sampling of weights equivalent to applying dropout operations. In our image retrieval setting, we apply dropout to all conventional layers of the feature extractor with a dropout rate  $p$ . Features  $\mu$  and their heuristic uncertainties  $\sigma^2$  are obtained by applying dropout at test time and feed forwarding  $T$  times:

$$\mu = \frac{1}{T} \sum_{t=1}^T f_{e_t \sim \theta}(X), \sigma^2 = \frac{1}{T} \sum_{t=1}^T (f_{e_t \sim \theta}(X) - \mu)^2. \quad (3)$$

where  $\theta$  denotes the weight posterior distribution.

**Uncertainty Estimated by an Ensemble** Ensemble method (Fort, Hu, and Lakshminarayanan 2019) trains multiple instances of the same deterministic model, each with random initial weights. During inference, predictions of all models are averaged, and the uncertainty is obtained as the variance of the predictions. Provided that there are  $N$  instances, the mean and variance of the predictions are:

$$\mu = \frac{1}{N} \sum_{i=1}^N f_{e_i}(X), \sigma^2 = \frac{1}{N} \sum_{i=1}^N (f_{e_i}(X) - \mu)^2. \quad (4)$$

### Uncertainty Estimated by a Single Deterministic Model

Multiple feed-forward propagations in MCD can cause overhead, and using multiple model instances can result in increased memory usage. In comparison, a single deterministic model is an attractive approach for estimating uncertainty. (Warburg et al. 2021) constructs a Gaussian distribution for each feature, i.e.,  $f_e(X) \sim \mathcal{N}(\mu, \sigma^2)$ . A Bayesian triplet loss is introduced to enforce contrastive learning among these probabilistic features. The network is built

upon a common image retrieval model by adding a variance head  $f_u$  parallel to the mean head  $f_e$ . Once trained, the model can output  $\mu$  and  $\sigma^2$  with one forward propagation:

$$[\mu, \sigma^2] = [f_e(X), f_u(X)]. \quad (5)$$

In summary, uncertainties of features are obtained by a BNN-based method, an ensemble or a single deterministic model. Nevertheless, the existing uncertainty-aware image retrieval methods are problematic in two senses:

1. They only provide a *heuristic* measure of uncertainty (Angelopoulos et al. 2022) rather than a guarantee. That said, even with the estimated uncertainty, the retrieval set *cannot* be interpreted with a likelihood of encompassing the true nearest neighbors of a given query sample.
2. The retrieval set’s uncertainty is represented by the query sample’s uncertainty (Warburg et al. 2021), which does not consider the retrieval set size. As a result, the same uncertainty value is assigned to a retrieval set with one sample as to a retrieval set with ten samples. However, a larger retrieval set has a higher likelihood of capturing the true nearest neighbors compared to a smaller one.

We propose RCIR to overcome these limitations: RCIR takes as input the user-specified risk level  $\alpha$  and error rate  $\delta$ , and outputs a risk-controlled retrieval set guaranteed to contain at least one true nearest neighbor of the query sample with a probability  $1 - \alpha$  and a error rate  $\delta$ . We describe RCIR in what follows.

### 3.3 Risk Controlled Image Retrieval

**Problem Setting** In RCIR, we denote the risk of an image retrieval system by  $\rho$ , which is the probability of the retrieval sets missing all true nearest neighbors of the query samples:

$$\rho(\mathcal{R}) = \mathbb{E}_{X \in \mathcal{Q}}[\ell(\mathcal{R}(X), \mathcal{S}(X))], \quad (6)$$

where  $\mathcal{R}$  denotes a generic retrieval function as in (2),  $\mathcal{S}(X)$  means retrieving all true nearest neighbors of  $X$ , and  $\ell$  indicates if the retrieval set misses all true nearest neighbors:

$$\ell(\mathcal{R}(X), \mathcal{S}(X)) = \mathbb{1}(\mathcal{R}(X) \cap \mathcal{S}(X) = \emptyset). \quad (7)$$

The risk function  $\rho(\cdot)$  evaluates the performance of a retrieval system  $\mathcal{R}$  on a query set  $\mathcal{Q}$ , and is bounded between 0 and 1.0:  $\rho(\mathcal{R}) = 0$  occurs when the retrieval set  $\mathcal{R}(X)$  covers at least one true nearest neighbor for all  $X$  in  $\mathcal{Q}$ , and  $\rho(\mathcal{R}) = 1.0$  happens when the retrieval set  $\mathcal{R}(X)$  never covers any true nearest neighbor for any  $X$  in  $\mathcal{Q}$ .

**Retrieval Set Size Adapter** In practice, end users will desire smaller retrieval sets for ‘easy’ query samples compared to ‘hard’ ones in order to save processing time, without sacrificing accuracy. To achieve this, we propose adapting the retrieval set size based on the query’s difficulty level. However, achieving this goal is not straightforward and has been barely explored in existing literature.

The first question we need to answer is: *what is the appropriate metric to measure a query’s difficulty level?* Our investigation shows that although existing heuristic uncertainties do not provide guarantees, they do correlate with

recall@1 (see Fig. 5). This discovery leads us to hypothesize that common heuristic uncertainty can serve as a coarse measure of a query’s difficulty level.

Moving on to the second question: *If such a metric exists, how to correlate the metric with the retrieval set size? what would be the principled way of building the relation between this metric and retrieval set size?* We have found a simple yet effective solution:

$$K_i = \lceil \kappa \cdot \Phi[f_u(X_i^{\mathcal{Q}})] \rceil, \quad (8)$$

where  $\kappa \in \mathbb{R}^+$  denotes the scale, which is computed by the `Controller` (will be explained soon),  $f_u$  is a heuristic uncertainty estimator,  $\Phi$  means normalizing the result to  $[0, 1]$ , and  $\lceil \cdot \rceil$  means rounding up to the nearest integer. The mapping function (8) presents the core function of the `Adapter`: adjust the retrieval set size based on the uncertainty of each query sample and a scale  $\kappa$ . With the `Adapter`, the image retrieval function in (1) is now conditioned on a varying retrieval set size  $K_i$ :

$$\{Y_{i,j} | j = 1, 2, \dots, K_i\} = \mathcal{R}_{[K_i, f_e]}(X_i^{\mathcal{Q}}). \quad (9)$$

**Risk Controller** Since  $f_u$  and  $f_e$  are fixed once an image retrieval model is trained, (8) indicates that the scale  $\kappa$  is the only parameter that can be tuned to proactively control the retrieval set size. Note that the `Adapter` alone cannot provide any risk guarantee for an image retrieval system. And we introduce the `Controller`, which computes the scale  $\kappa$  such that the risk is controlled.

**Lemma 3.1.** *Given a dataset  $\{\mathcal{Q}, \mathcal{D}\}$ , let the pretrained feature extractor  $f_e$  and uncertainty estimator  $f_u$  be fixed, then the risk function  $\rho(\mathcal{R}_{[\kappa, f_u, f_e]})$  is a monotone nonincreasing function of the  $\kappa$  for  $\forall \kappa \in \mathbb{R}^+$ .*

*Proof.* For any  $i^{\text{th}}$  query  $X_i^{\mathcal{Q}}$ , if  $\kappa_1 > \kappa_2$ , then  $K_{i, \kappa_1} \geq K_{i, \kappa_2}$  (by mapping function (8) as  $f_u$  is fixed), which means  $|\mathcal{R}_{[\kappa_1, f_u, f_e]}(X_i^{\mathcal{Q}})| \geq |\mathcal{R}_{[\kappa_2, f_u, f_e]}(X_i^{\mathcal{Q}})|$ .

Since in a retrieval system, the candidates are retrieved based on a consistent distance metric  $d$  (see (2)),

$$\mathcal{R}_{[\kappa_2, f_u, f_e]}(X_i^{\mathcal{Q}}) \subseteq \mathcal{R}_{[\kappa_1, f_u, f_e]}(X_i^{\mathcal{Q}}).$$

Then, by the loss definition in (7),

$$\ell(\mathcal{R}_{[\kappa_2, f_u, f_e]}(X_i^{\mathcal{Q}}), \mathcal{S}(X_i^{\mathcal{Q}})) \geq \ell(\mathcal{R}_{[\kappa_1, f_u, f_e]}(X_i^{\mathcal{Q}}), \mathcal{S}(X_i^{\mathcal{Q}})),$$

and thus, by the risk definition in (6),

$$\rho(\mathcal{R}_{[\kappa_2, f_u, f_e]}) \geq \rho(\mathcal{R}_{[\kappa_1, f_u, f_e]}).$$

□

In a trained image retrieval system,  $f_u$  and  $f_e$  remain fixed while the representation  $\rho(\mathcal{R}_{[\kappa, f_u, f_e]})$  only changes with  $\kappa$ . Thereafter, we will refer to this representation as  $\rho(\kappa)$ .

**Theorem 3.2.** *Assume for each  $\kappa$  the risk  $\rho(\kappa)$  is a monotone nonincreasing function, and an upper confidence bound of the risk, which we denote by  $\hat{\rho}^+(\kappa)$ , is accessible. If  $\forall \kappa \in \mathbb{R}^+$ ,*

$$P(\rho(\kappa) \leq \hat{\rho}^+(\kappa)) \geq 1 - \delta, \quad (10)$$

---

Algorithm 1: Compute  $\hat{\kappa}$ .

---

**Input:** Calibration set  $\{\mathcal{Q}', \mathcal{D}'\}$ , risk level  $\alpha$ , error rate  $\delta$ , trained feature extractor  $f_e$ , trained heuristic uncertainty estimator  $f_u$

**Output:**  $\hat{\kappa}$

```

1:  $\kappa \leftarrow 1, \hat{\rho}^+(\kappa) \leftarrow 1$ 
2: while  $\hat{\rho}^+(\kappa) > \alpha$  do
3:    $\kappa = \kappa + \Delta\kappa$ 
4:   for  $i$  in  $1, 2, \dots, |\mathcal{Q}'|$  do
5:      $K_i = \lceil \kappa \cdot \Phi[f_u(X_i^{\mathcal{Q}'})] \rceil$ 
6:      $l_i = \mathbb{1}[\mathcal{R}_{[K_i, f_e]}(X_i^{\mathcal{Q}'}) \cap \mathcal{S}(X_i^{\mathcal{Q}'}) = \emptyset]$ 
7:   end for
8:    $\hat{\rho}(\kappa) = \frac{1}{|\mathcal{Q}'|} \sum_i |\mathcal{Q}'| l_i$ 
9:    $\hat{\rho}^+(\kappa) = \hat{\rho}(\kappa) + \sqrt{\frac{1}{2n} \log \frac{1}{\delta}}$ 
10: end while
11:  $\hat{\kappa} = \kappa - \Delta\kappa$ 
12: return  $\hat{\kappa}$ 

```

---

and let  $\hat{\kappa}$  denotes the smallest  $\kappa$  such that for any  $\kappa > \hat{\kappa}$  we have  $\hat{\rho}^+(\kappa) \leq \alpha$ , i.e.,

$$\hat{\kappa} = \inf\{\kappa : \hat{\rho}^+(\kappa) \leq \alpha, \forall \kappa' > \kappa\}, \quad (11)$$

then

$$P(\rho(\hat{\kappa}) \leq \alpha) \geq 1 - \delta. \quad (12)$$

*Proof.* Let  $\kappa^*$  be the smallest value of  $\kappa$  that ensures the risk is less than  $\alpha$ , as given by the equation:

$$\kappa^* = \inf\{\kappa : \rho(\kappa) \leq \alpha\}, \quad (13)$$

then, due to the continuity of  $\rho(\kappa)$ , it follows that  $\rho(\kappa^*) = \alpha$ . Fig. 3 provides an visualization of  $\rho$ .

We define two events: event  $A$ , which is when  $\rho(\hat{\kappa}) > \alpha$ , and event  $B$ , which is when  $\rho(\kappa^*) > \hat{\rho}^+(\kappa^*)$ . It can be proven that  $A$  is a sufficient condition for  $B$ . This is because if  $\rho(\hat{\kappa}) > \alpha$ , then  $\hat{\kappa} < \kappa^*$  (due to the monotonicity of  $\rho(\kappa)$ ), which implies  $\hat{\rho}^+(\kappa^*) < \alpha$  (according to (11) and ). Since  $\rho(\kappa^*) = \alpha$  and  $\hat{\rho}^+(\kappa^*) < \alpha$ , it follows that  $\rho(\kappa^*) > \hat{\rho}^+(\kappa^*)$ . As  $A$  is a sufficient condition for  $B$ ,  $P(A) \leq P(B)$ . According to (10),  $P(B) < \delta$ , and therefore,  $P(A) < \delta$ . Consequently,  $P(\bar{A}) \geq 1 - \delta$ , i.e.,  $P(\rho(\hat{\kappa}) \leq \alpha) \geq 1 - \delta$ .  $\square$

With (11), we can proceed to determine an upper confidence bound  $\hat{\rho}^+(\kappa)$ . According to (Bates et al. 2021), Hoeffding’s inequality is applicable to our risk function  $\rho(\kappa)$ , which is bounded by one. We denote the risk on the calibration set by  $\hat{\rho}(\kappa)$ . Hoeffding’s inequality indicates

$$P(\hat{\rho}(\kappa) - \rho(\kappa) \leq -x) \leq e^{-2nx^2}, \quad (14)$$

which implies upper confidence bound

$$\hat{\rho}^+(\kappa) = \hat{\rho}(\kappa) + \sqrt{\frac{1}{2n} \log \left( \frac{1}{\delta} \right)}. \quad (15)$$

Given a predefined risk requirement, i.e., risk level  $\alpha$  and error rate  $\delta$ , the Controller uses (11) to compute  $\hat{\kappa}$ . The

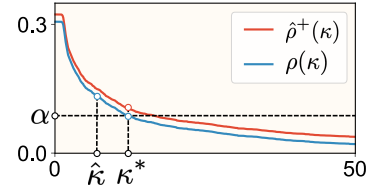


Figure 3: The  $\rho - \kappa$  curve on the CAR-196 calibration set: the risk  $\rho(\kappa)$  is monotone nonincreasing with  $\kappa$ .

computation process is outlined in Algorithm 1. Once  $\hat{\kappa}$  is obtained, the Adapter generates the retrieval set size  $K_i$ , and the image retrieval function retrieves the risk-controlled retrieval set, which is ensured to have at least one true nearest neighbor with a probability of  $1 - \alpha$ , and that the chance of the assert fail is limited to  $\delta$ .

## 4 Experiments

### 4.1 Datasets

**CUB-200** (Wah et al. 2011) contains 11,788 images of 200 classes. Each class has at least 50 images. We use the first 100 classes as a training set and the other 100 as a test set.

**Stanford CAR-196** Stanford CAR-196 (Krause et al. 2013) contains 16,185 images of 196 classes. Each class has at least 80 images. We use the first 98 classes as the training set and the other 98 classes as the test set.

**Pittsburgh** (Torii et al. 2013) is a large image database from Google Street View. Following the split of NetVLAD (Arandjelovic et al. 2016), we adopt the subset that consists of 10k samples in the training/validation/test split.

**ChestX-Det** (Lian et al. 2021) is a subset of the public dataset NIH ChestX-ray14, and it contains 3543 images with 14 classes (13 categories of diseases and normal cases). We choose samples of the six classes as the training set, and the rest as the test set.

For all datasets, we randomly choose 50% images from the test set to form the calibration set.

### 4.2 Implementations

RCIR is versatile and can be applied to any image retrieval system that provides heuristic uncertainty. To show the effectiveness of RCIR, we first build three conventional image retrieval systems based on (Warburg et al. 2021): **BTL**, **MCD** and **Deep Ensemble**, each of which has a feature extractor and an uncertainty estimator as described in Sec.3.2. BTL, MCD and Deep Ensemble retrieve fixed  $K$  database samples when given a query. For comparing purposes, we also include a **Deterministic** image retrieval system that only has a feature extractor.

All models are trained using the Adam optimizer with an initial learning rate of  $10^{-5}$  and an exponential learning rate scheduler with gamma 0.99. The weight decay is set to  $10^{-3}$ . The feature dimension is 2048, and the variance dimension is 1. We adopt a hard mining strategy and feed the model with triplets that violate the triplet margin (Warburg et al. 2021). We refer readers to the Appendix for the details of the network and training details.



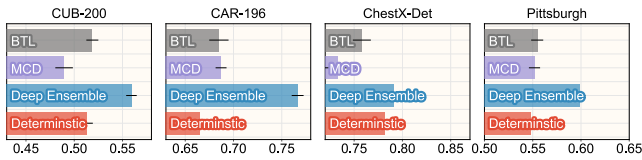


Figure 4: The Recall@1 results of different methods on various test sets. The error bars represent the standard deviation of the results of 10 trials.

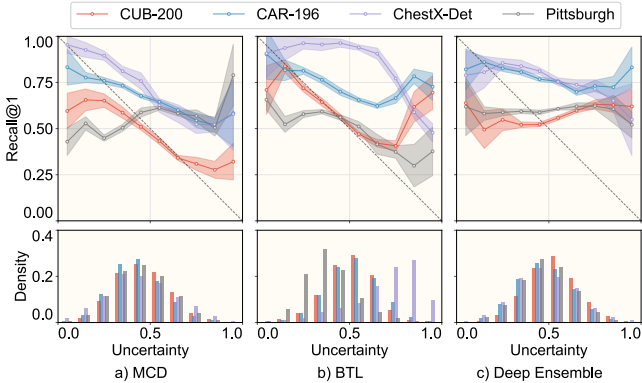


Figure 5: The reliability diagrams of different methods on different test sets. The dashed line denotes the ideally-calibrated line. The colored shadows represent the standard deviation of the results of 10 trials.

### 4.3 Metrics

We first follow the common evaluation steps (Warburg et al. 2021) for image retrieval systems, use **recall@1** to evaluate the retrieval performance of the feature extractor and **reliability diagram** (Guo et al. 2017) to assess the uncertainty quality of the uncertainty estimator. Then, we use **empirical risk**, which is the risk calculated on the test set, to evaluate the risk control performance. In addition, **retrieval set size** is used to examine that RCIR does not resort to large retrieval sets to lower the empirical risk. The retrieval set size should be minimized while the risk is controlled. Because large retrieval sets tend to include more negative samples and are inefficient for downstream processing. We also provide **qualitative visualization** to show more insights into the image retrieval system. Please refer to the Appendix for details of these metrics.

### 4.4 Results

We first analyze the results of the three conventional image retrieval systems, in terms of image retrieval performance and uncertainty calibration.

**Recall@1 (image retrieval performance)** We begin by evaluating the retrieval performance of various methods. The Recall@1 of different image retrieval systems on various test sets are presented in Fig. 4. BTL achieves a higher recall@1 than Deterministic on most datasets, suggesting that a feature extractor can benefit from uncertainty-aware training. Nevertheless, MCD’s performance is inconsistent

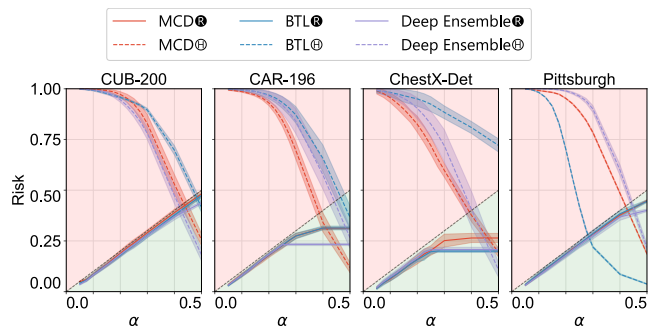


Figure 6: The risks on different test sets: risk is well controlled by RCIR (see  $\times \textcircled{R}$ ) under different risk levels  $\alpha$  (with  $\delta = 0.1$ ). The colored shadows represent the standard deviation of the results of 10 trials.

when compared to Deterministic, which may be due to the impact of the dropout layers on the representation power, depending on the dataset scale. Deep Ensemble achieves the best performance, which can be attributed to the fact that it utilizes multiple models to average out noises.

**Reliability diagram (uncertainty estimation performance)** Fig. 5 depicts the reliability diagrams of the uncertainty estimator in different image retrieval systems across the four datasets. It can be seen that none of these curves conforms to the ideally-calibrated line, indicating that the heuristic uncertainty itself is not reliable. Moreover, the gaps between the curves and the dashed line vary across datasets for both MCD, BTL and Deep Ensemble, implying that the same uncertainty estimation method cannot consistently perform across different datasets.

Next, we build RCIR by plugging our *Adapter* and *Controller* modules into conventional image retrieval systems. We denote the three RCIR systems as **BTL $\textcircled{R}$** , **MCD $\textcircled{R}$**  and **Deep Ensemble $\textcircled{R}$** . Meanwhile, to evaluate the practical usefulness of heuristic uncertainty, we normalize heuristic uncertainties to the range  $[0, 1]$  based on their statistics on the calibration set. Then each query-candidate pair’s uncertainty is calculated as the sum of their individual uncertainties (Warburg et al. 2021). This will result in three comparing methods: **BTL $\textcircled{\oplus}$** , **MCD $\textcircled{\oplus}$**  and **Deep Ensemble $\textcircled{\oplus}$** . For fairness,  $\times \textcircled{R}$  will retrieve as many candidates as  $\times \textcircled{\oplus}$  can achieve, then only pairs with uncertainties below  $1 - \alpha$  will be kept.

**Empirical risk (risk control performance)** Fig. 6 shows the empirical risk of different image retrieval systems on different datasets. It can be observed that the risks of  $\times \textcircled{R}$  are always below the predefined risk levels  $\alpha$ . This means that even before retrieval we can say for sure that the retrievals of  $\times \textcircled{R}$  have a  $1 - \alpha$  probability of covering the true nearest neighbors, with only a  $\delta$  probability of being wrong. In comparison, the heuristic uncertainty-only methods, including MCD $\textcircled{\oplus}$ , BTL $\textcircled{\oplus}$  and Deep Ensemble $\textcircled{\oplus}$  exhibit risks higher than the predefined risk levels in the range  $\alpha < 0.4$ . The results show that the heuristic uncertainty alone is not reliable to be used for risk control, while RCIR can control

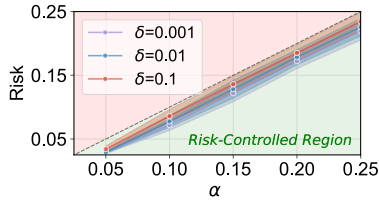


Figure 7: The risks on the Pittsburgh test set with different error rates by BTL<sup>Ⓡ</sup>: smaller  $\delta$  leads to more conservative retrievals (e.g., larger retrieval size). The colored shadows represent the standard deviation of the results of 10 trials.

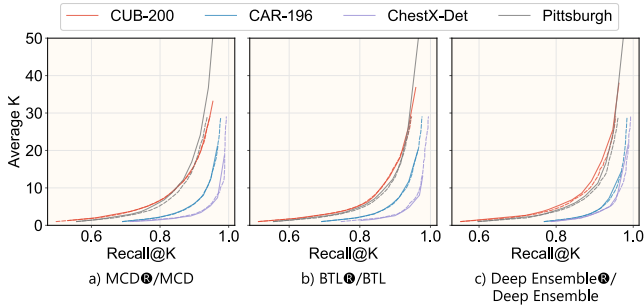


Figure 8: The average  $K$  across different methods on different test sets (*solid line* — means  $\times^{\text{R}}$  (with  $\delta = 0.1$ ), while *dashed line* - - - means their conventional counterparts): When achieving the same recall,  $\times^{\text{R}}$  and their conventional counterparts have similar average retrieval set sizes, indicating that the adaptive strategy does not rely on simply increasing  $K$  to control the risk.

the risk well.

In addition, we investigate the effect of using different  $\delta$ , which controls how conservative the RCIR is. Fig. 2 shows the empirical risk with different  $\delta$  on the Pittsburgh dataset. With a smaller  $\delta$ , RCIR would be more conservative (i.e., larger retrieval size) to ensure the risk is below the given  $\alpha$ . Similar trends can be observed on other datasets (see Fig. 2 in the Appendix for results on more datasets).

**Retrieval set size** RCIR may always resorts to large retrieval sets to lower the empirical risk, in which situation the risk is trivially controlled but the retrieval sets would be of less practical use. To examine this, we compare MCD<sup>Ⓡ</sup>, BTL<sup>Ⓡ</sup> and Deep Ensemble<sup>Ⓡ</sup> against their fix-size retrieval counterparts. Fig. 8 shows that when achieving the same recall@ $K$ ,  $\times^{\text{R}}$  and their fix-size retrieval counterparts have similar average retrieval set sizes. This indicates that  $\times^{\text{R}}$  does not rely on simply increasing  $K$  to control the risk. But we also notice that MCD<sup>Ⓡ</sup> and Deep Ensemble<sup>Ⓡ</sup> on the Pittsburgh test set have a slightly larger average retrieval set size than their fix-size retrieval counterparts. This is likely due to poor uncertainty estimation on the Pittsburgh test set, as shown in Fig. 5.

**Qualitative visualization** The distribution of retrieval size on the Pittsburgh test set is presented in Fig. 3 (see Fig. 3 in the Appendix for results on more datasets). It is evident that

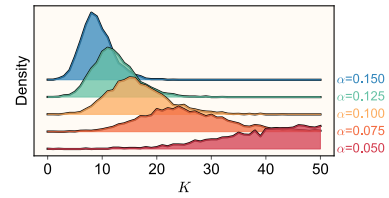


Figure 9: The retrieval size,  $K$ , on the Pittsburgh test set by BTL<sup>Ⓡ</sup>: retrieval set size adapts to the risk level  $\alpha$ . ( $\delta = 0.1$ )

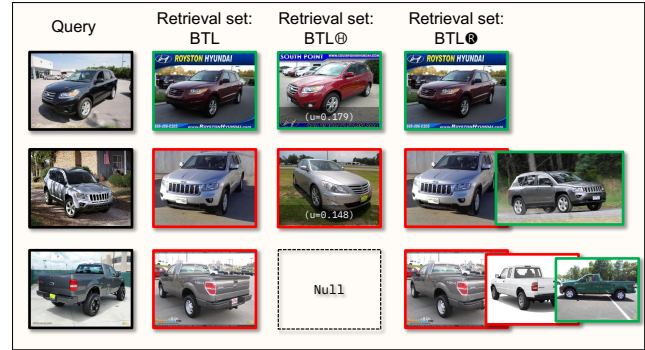


Figure 10: The qualitative visualization of retrieval sets on the CAR-196 test set by different methods (Red border  $\square$  denotes a wrong candidate, while green border  $\square$  correct): BTL<sup>Ⓡ</sup> adjusts the size of retrievals to reflect the uncertainty while ensuring coverage ( $\alpha = 0.2$  and  $\delta = 0.1$ ).

the retrieval size varies with the risk level  $\alpha$ : a smaller  $\alpha$  results in a larger retrieval size, and vice versa. This helps end users save time on easy queries and focus on more difficult ones. Fig. 10 shows the qualitative visualization of retrievals on the CAR-196 dataset by different methods. In the first row, it is evident that when a relatively easy query is provided, all methods successfully retrieve the correct results. Moving on to the second row, where the query is more challenging, the fixed-size retrieval method fails without any indication, and BTL<sup>Ⓡ</sup> fails as well with a low heuristic number. However, BTL<sup>Ⓡ</sup> takes into account the difficulty of the query and retrieves an additional candidate, resulting in the correct answer. The third row represents a more demanding query. BTL<sup>Ⓡ</sup> generates no candidate, while BTL<sup>Ⓡ</sup> retrieves more candidates to meet the coverage requirement.

## 5 Conclusion

We present RCIR, a significant improvement to the current uncertainty-aware image retrieval systems. Unlike the heuristic uncertainty provided by existing methods, RCIR offers a coverage guarantee. We include a theoretical analysis of the risk bound of RCIR and present extensive experimental results, which demonstrate its efficacy in controlling the risk of existing image retrieval systems. We believe that the advancement made by RCIR can benefit risk-sensitive applications, such as medical diagnosis and autonomous driving.

## References

- Angelopoulos, A. N.; Kohli, A. P.; Bates, S.; Jordan, M.; Malik, J.; Alshaabi, T.; Upadhyayula, S.; and Romano, Y. 2022. Image-to-image regression with distribution-free uncertainty quantification and applications in imaging. In *International Conference on Machine Learning*, 717–730. PMLR.
- Arandjelovic, R.; Gronat, P.; Torii, A.; Pajdla, T.; and Sivic, J. 2016. NetVLAD: CNN architecture for weakly supervised place recognition. In *Proceedings of the IEEE conference on computer vision and pattern recognition*, 5297–5307.
- Babenko, A.; Slesarev, A.; Chigorin, A.; and Lempitsky, V. 2014. Neural codes for image retrieval. In *Computer Vision—ECCV 2014: 13th European Conference, Zurich, Switzerland, September 6–12, 2014, Proceedings, Part I 13*, 584–599. Springer.
- Bates, S.; Angelopoulos, A.; Lei, L.; Malik, J.; and Jordan, M. 2021. Distribution-free, risk-controlling prediction sets. *Journal of the ACM (JACM)*, 68(6): 1–34.
- Chang, J.; Lan, Z.; Cheng, C.; and Wei, Y. 2020. Data uncertainty learning in face recognition. In *Proceedings of the IEEE/CVF conference on computer vision and pattern recognition*, 5710–5719.
- Cheng, Y.; and Wang, H. 2019. A modified contrastive loss method for face recognition. *Pattern Recognition Letters*, 125: 785–790.
- Dubey, S. R. 2022. A Decade Survey of Content Based Image Retrieval Using Deep Learning. *IEEE Transactions on Circuits and Systems for Video Technology*, 32(5): 2687–2704.
- Fort, S.; Hu, H.; and Lakshminarayanan, B. 2019. Deep ensembles: A loss landscape perspective. *arXiv preprint arXiv:1912.02757*.
- Gal, Y.; and Ghahramani, Z. 2016. Dropout as a bayesian approximation: Representing model uncertainty in deep learning. In *international conference on machine learning*, 1050–1059. PMLR.
- Guo, C.; Pleiss, G.; Sun, Y.; and Weinberger, K. Q. 2017. On Calibration of Modern Neural Networks. In *International Conference on Machine Learning (ICML)*, 1321–1330.
- Hadsell, R.; Chopra, S.; and LeCun, Y. 2006. Dimensionality reduction by learning an invariant mapping. In *2006 IEEE Computer Society Conference on Computer Vision and Pattern Recognition (CVPR'06)*, volume 2, 1735–1742. IEEE.
- He, K.; Zhang, X.; Ren, S.; and Sun, J. 2016. Deep residual learning for image recognition. In *Proceedings of the IEEE conference on computer vision and pattern recognition*, 770–778.
- Kendall, A.; and Gal, Y. 2017. What uncertainties do we need in bayesian deep learning for computer vision? *Advances in neural information processing systems*, 30.
- Krause, J.; Stark, M.; Deng, J.; and Fei-Fei, L. 2013. 3d object representations for fine-grained categorization. In *Proceedings of the IEEE international conference on computer vision workshops*, 554–561.
- Lian, J.; Liu, J.; Zhang, S.; Gao, K.; Liu, X.; Zhang, D.; and Yu, Y. 2021. A structure-aware relation network for thoracic diseases detection and segmentation. *IEEE Transactions on Medical Imaging*, 40(8): 2042–2052.
- Lowe, D. G. 1999. Object recognition from local scale-invariant features. In *Proceedings of the seventh IEEE international conference on computer vision*, volume 2, 1150–1157. Ieee.
- Radenović, F.; Tolias, G.; and Chum, O. 2018. Fine-tuning CNN image retrieval with no human annotation. *IEEE transactions on pattern analysis and machine intelligence*, 41(7): 1655–1668.
- Romano, Y.; Patterson, E.; and Candes, E. 2019. Conormalized quantile regression. *Advances in neural information processing systems*, 32.
- Schroff, F.; Kalenichenko, D.; and Philbin, w. c. d. t. r. . h. o. o. w. a. p. o. a. m. d. m., JaUsing (10). 2015. Facenet: A unified embedding for face recognition and clustering. In *Proceedings of the IEEE conference on computer vision and pattern recognition*, 815–823.
- Sohn, K. 2016. Improved deep metric learning with multi-class n-pair loss objective. *Advances in neural information processing systems*, 29.
- Taha, A.; Chen, Y.-T.; Yang, X.; Misu, T.; and Davis, L. 2019. Exploring uncertainty in conditional multi-modal retrieval systems. *arXiv preprint arXiv:1901.07702*.
- Torii, A.; Sivic, J.; Pajdla, T.; and Okutomi, M. 2013. Visual place recognition with repetitive structures. In *Proceedings of the IEEE conference on computer vision and pattern recognition*, 883–890.
- Vovk, V.; Gammerman, A.; and Shafer, G. 2005. *Algorithmic learning in a random world*, volume 29. Springer.
- Wah, C.; Branson, S.; Welinder, P.; Perona, P.; and Belongie, S. 2011. The caltech-ucsd birds-200-2011 dataset.
- Warburg, F.; Jørgensen, M.; Civera, J.; and Hauberg, S. 2021. Bayesian triplet loss: Uncertainty quantification in image retrieval. In *Proceedings of the IEEE/CVF International conference on Computer Vision*, 12158–12168.
- Yao, H.; Zhang, S.; Hong, R.; Zhang, Y.; Xu, C.; and Tian, Q. 2019. Deep representation learning with part loss for person re-identification. *IEEE Transactions on Image Processing*, 28(6): 2860–2871.
- Zhang, Y.; Wang, C.; and Deng, W. 2021. Relative uncertainty learning for facial expression recognition. *Advances in Neural Information Processing Systems*, 34: 17616–17627.



## A Implementations

### A.1 Network Architectures

Figure 1 illustrates the network architectures of the three image retrieval models used in our experiments:

- The **Deterministic** model is composed of ResNet-50 (He et al. 2016) backbone, a GeM layer (Radenović, Tolias, and Chum 2018), a fully connected layer and a L2-normalization layer. The Deterministic model is trained with the triplet loss (Schroff, Kalenichenko, and Philbin 2015).
- The **MCD** model is the same as the Deterministic except that we apply dropout to all conventional layers of the backbone during both training and testing time.
- The **BTL** model has an additional variance head, and it is trained with the Bayesian triplet loss (Warburg et al. 2021).
- The **Deep Ensemble** is built with 5 Deterministic models.

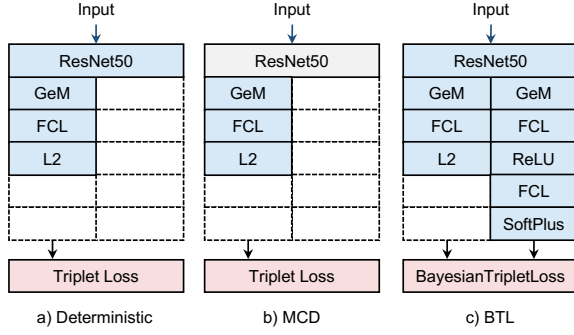


Figure 1: The network architectures of different image retrieval models.

### A.2 Loss Functions

**Bayesian Triplet Loss** Bayesian triplet loss was proposed in (Warburg et al. 2021), and we include it here for completeness. In this setting, embeddings are modeled as a Gaussian distribution  $\mathcal{N}(f_\phi(X), f_\sigma^2(X))$ . Denote embeddings of query, positive, and negative images as  $q$ ,  $p$ , and  $n$ , respectively. The probability that a query is closer to a positive than a negative is

$$P(\|a - p\|^2 - \|a - n\|^2 < -m), \quad (1)$$

where  $m$  is a predefined margin. (1) is equivalent to

$$P(\tau < -m), \quad (2)$$

where  $\tau = \sum_{d=1}^D (a_d - p_d)^2 - (a_d - n_d)^2$ , and  $D$  is the dimension of the embedding. Since  $\tau$  will approximate a Gaussian distribution when  $D$  is large, we can obtain the

leading two moments of  $\tau$  as

$$\begin{aligned} \mu &= \mu_p^2 + \sigma_p^2 - \mu_n^2 - \sigma_n^2 - 2\mu_a(\mu_p - \mu_n), \\ \sigma^2 &= 2[\sigma_p^4 + 2\mu_p^2\sigma_p^2 + 2(\sigma_a^2 + \mu_a^2)(\sigma_p^2 + \mu_p^2) - 2\mu_a^2\mu_p^2 \\ &\quad - 4\mu_a\mu_p\sigma_p^2] + 2[\sigma_n^4 + 2\mu_n^2\sigma_n^2 + 2(\sigma_a^2 + \mu_a^2)(\sigma_n^2 + \mu_n^2) \\ &\quad - 2\mu_a^2\mu_n^2 - 4\mu_a\mu_n\sigma_n^2] - 8\mu_p\mu_n\sigma_a^2. \end{aligned} \quad (3)$$

The loss is obtained as

$$\mathcal{L}_{BTL} = -\frac{1}{T} \sum_{t=1}^T \log P(\tau < -m), \quad (4)$$

where  $T$  is the number of triplets in a batch.

**Triplet Loss** In the triplet loss (Schroff, Kalenichenko, and Philbin 2015) setting, we denote embeddings of query, positive, and negative images as  $q$ ,  $p$ , and  $n$ , respectively.

$$\mathcal{L}_{TL} = \frac{1}{T} \sum_{t=1}^T \max(0, \|a - p\|^2 - \|a - n\|^2 + m), \quad (5)$$

where  $T$  is the number of triplets in a batch,  $m$  is a predefined margin.

When training Deterministic, MCD and BTL models, we follow (Warburg et al. 2021) and use online hardest mining to generate triplet tuples. Specifically, we first randomly select a query image  $X_i^q$ . Then, we select a positive image  $X_i^p$  from the same class that has the largest embedding distance to the query image as  $X_i^q$ . Finally, we select a batch of negative images  $\{X_{i,1}^n, X_{i,2}^n, \dots, X_{i,J}^n\}$  from a different class that has the smallest embedding distance to the query. We refresh the embedding cache before every epoch.

### A.3 Metrics

- **Recall@1**: The Recall@1 is the percentage of queries whose top-1 retrieved sample is the true nearest neighbor of the query.
- **Reliability diagram**: Given finite query samples, the trained uncertainty estimator estimates the uncertainty for each query sample. These uncertainties are then normalized to fit within the range of  $[0, 1.0]$  (Warburg et al. 2021). We organize the query samples into 10 bins based on their uncertainties, grouping them into intervals such as  $[0, 0.1)$ ,  $[0.1, 0.2)$ , ...,  $[0.9, 1.0]$ . By calculating the recall@1 for the query samples in each bin, we can evaluate how well the uncertainty estimator is calibrated. Ideally, we expect the recall@1 to decrease proportionally with the uncertainty, as depicted by the dashed line in the reliability diagram.

## B Experimental Results

Fig. 2 shows the empirical risk with different  $\delta$  on the different test sets. With a smaller  $\delta$ , RCIR would be more conservative (i.e., larger retrieval size) to ensure the risk is below the given  $\alpha$ .

Fig. 3 presents the distribution of retrieval size on different test sets. It is evident that the retrieval size varies with the risk level  $\alpha$ : a smaller  $\alpha$  results in a larger retrieval size, and vice versa. This helps end users save time on easy queries and focus on more difficult ones.

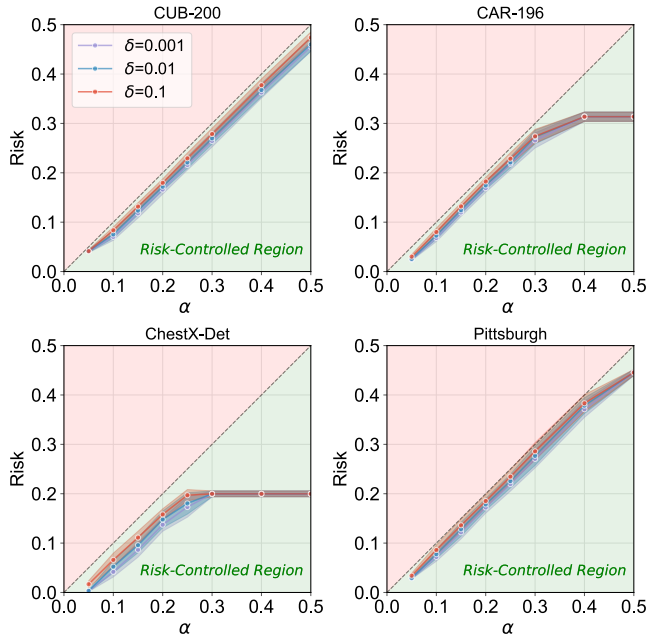


Figure 2: The risks on different test sets with different error rates by BTL<sup>®</sup>: smaller  $\delta$  leads to more conservative retrievals (e.g., larger retrieval size). The colored shadows represent the standard deviation of the results of 10 trials.

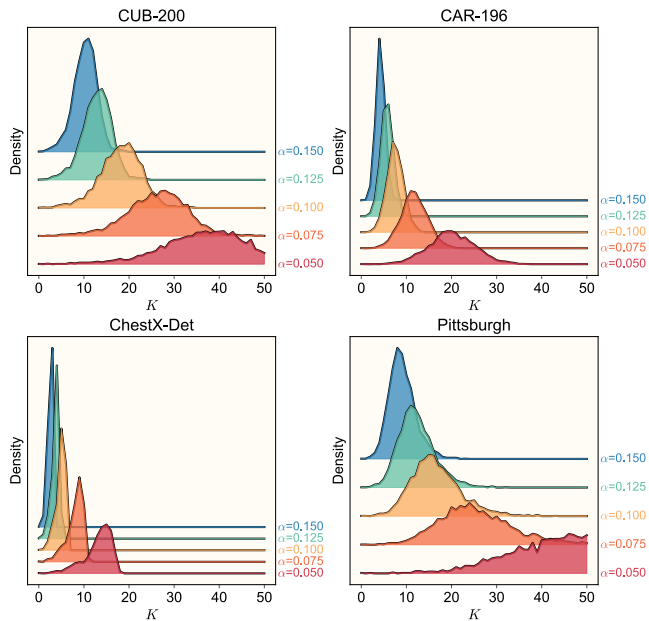


Figure 3: The retrieval size,  $K$ , on different test sets by BTL<sup>®</sup>: retrieval set size adapts to the risk level  $\alpha$ .